

PAPER

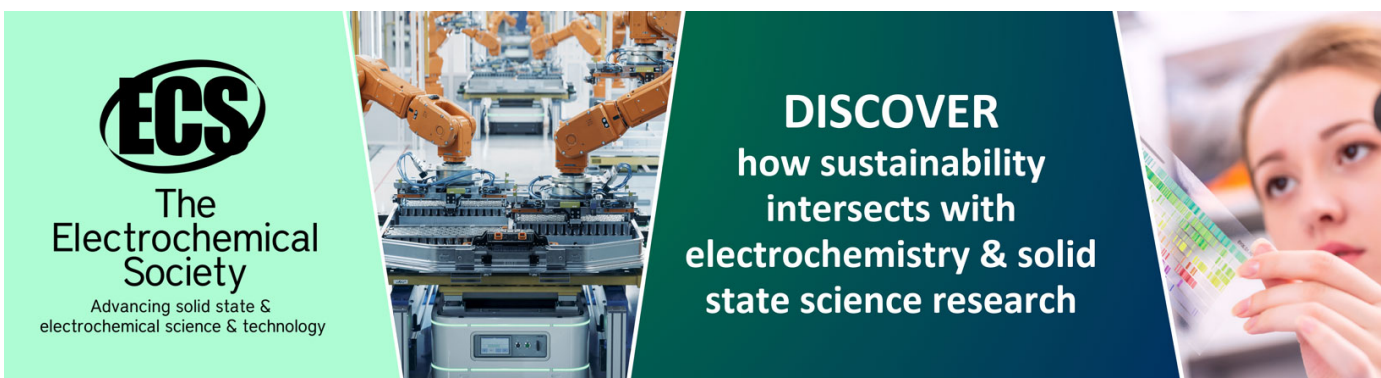
Upconverting crystal/dextran-g-DOPE with high fluorescence stability for simultaneous photodynamic therapy and cell imaging

To cite this article: HanJie Wang *et al* 2014 *Nanotechnology* **25** 155103

View the [article online](#) for updates and enhancements.

You may also like

- [Self-assembly of an upconverting nanocomplex and its application to turn-on detection of metalloproteinase-9 in living cells](#)
Phuong-Diem Nguyen, Vu Thanh Cong, Changyoon Baek *et al.*
- [Inorganic nanocarriers for siRNA delivery for cancer treatments](#)
Ganeshlenin Kandasamy and Dipak Maity
- [Targeted polyethylenimine/\(p53 plasmid\) nanocomplexes for potential antitumor applications](#)
Yuan Zhong, Yi Wang, Li Luo *et al.*



ECS
The
Electrochemical
Society
Advancing solid state &
electrochemical science & technology

DISCOVER
how sustainability
intersects with
electrochemistry & solid
state science research

Upconverting crystal/dextran-g-DOPE with high fluorescence stability for simultaneous photodynamic therapy and cell imaging

HanJie Wang¹, Sheng Wang¹, Zhongyun Liu¹, Chunhong Dong¹, Jiumin Yang², Xiaoqun Gong³ and Jin Chang¹

¹ Institute of Nanobiotechnology, School of Materials Science and Engineering, Tianjin University and Tianjin Key Laboratory of Composites and Functional Materials, Tianjin 300072, People's Republic of China

² School of Biomedical Engineering, Tianjin Medical University, Tianjin 300070, People's Republic of China

³ School of Life Sciences, Tianjin University, Tianjin 300072, People's Republic of China

E-mail: jinchang@tju.edu.cn

Received 11 November 2013, revised 20 January 2014

Accepted for publication 29 January 2014

Published 20 March 2014

Abstract

To date, the application of photodynamic therapy in deep tissue has been severely restricted by the limited penetration depth of excitation light, such as UV light and visible light. In this work, a protocol of upconverting crystal/dextran-g-DOPE nanocomplex (UCN/dextran-g-DOPE) was developed. The nanocomplex was assembled from the hydrophobic upconverting nanoparticle (UCN) core and hydrophilic lipid shell. The photosensitizer zinc phthalocyanine (ZnPc) loaded UCN/dextran-g-DOPE offers possibilities to overcome the problem mentioned above. The UCN core works as a transducer to convert deeply penetrating near-infrared light to visible light to activate ZnPc for photodynamic therapy. The dextran-g-DOPE lipid shell is used for loading ZnPc and protecting the whole system from nonspecific absorbance or corrosion during the transportation. The experiment results show that the nanocomplex is an individual sphere with an average size of 30 nm. The ZnPc was activated to produce singlet oxygen successfully by the upconverting fluorescence emitted from UCN. The nanocomplex has high fluorescence stability in alkaline or neutral buffer solutions. Importantly, the ZnPc loaded UCN/dextran-g-DOPE nanocomplex showed a significant inhibitory effect on tumor cells after NIR exposure. Our data suggest that a ZnPc loaded UCN/dextran-g-DOPE nanocomplex may be a useful nanoplatform for future PDT treatment in deep-cancer therapy based on the upconverting mechanism.

Keywords: upconverting nanocrystal, dextran, polymeric lipid, nanocomplex, photodynamic therapy

 Online supplementary data available from stacks.iop.org/Nano/25/155103/mmedia

(Some figures may appear in colour only in the online journal)

1. Introduction

Photodynamic therapy (PDT), an emerging treatment strategy, is used clinically to treat a wide range of medical conditions, especially malignant cancers [1, 2]. PDT is considered

to be both minimally invasive and minimally toxic which makes it an attractive alternative to surgery, chemotherapy and actinotherapy [3]. PDT involves three key components: the photosensitizer, light, and tissue oxygen. Upon the excitation by light of a suitable wavelength, photosensitizer molecules

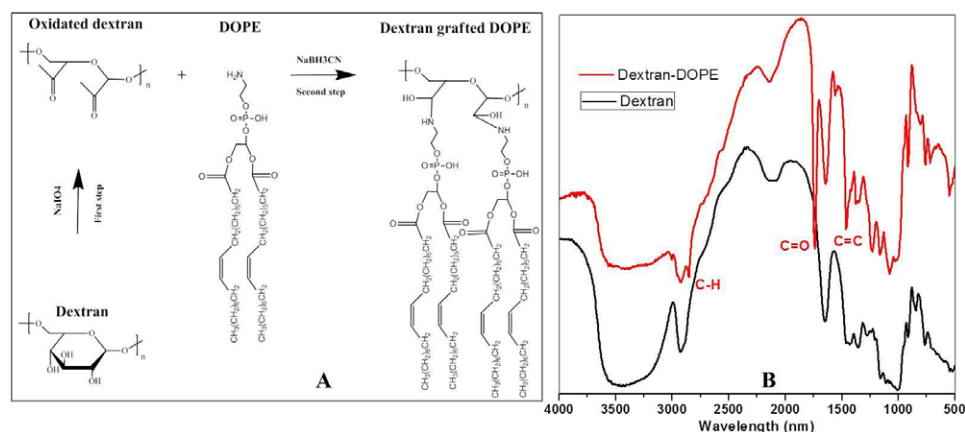


Figure 1. (A) The synthesis process of dextran-grafted DOPE; (B) FTIR spectrum of dextran and dextran-g-DOPE.

transfer the absorbed photon energy to oxygen molecules in the surroundings, generating cytotoxic reactive oxygen species (ROS) to kill cancer cells [4, 5]. However, most photosensitizers are excited by visible or even UV light, which has limited penetration depth due to the light absorption of the biological tissues, resulting in ineffective therapeutic effects to internal or large tumors [6, 7]. To date, PDT is limited to treating tumors on or just under the skin or on the lining of internal organs or cavities and is less effective when treating large and deep-seated tumors [8]. Solving this problem will directly influence the further application of PDT in cancer treatment.

As is known, the body is relatively transparent to near-infrared (NIR) light in the range of 700–1000 nm. NIR light of 650–900 nm can penetrate up to 10 cm into living tissue, which makes it ideal for optical imaging and phototherapy [9–12]. So the use of NIR light in PDT can afford greater penetration depths than that of vis light. NIR-to-vis upconverting nanoparticles (UCNs), which convert two or more low-energy pump photons from the NIR spectral region to a higher-energy output photon with a shorter wavelength, have been developed for applications in biological labeling, sensing and imaging. In the biological treatment field, the visible light emitted from UCNs after NIR exposure can excite the photosensitizers to produce singlet oxygen for PDT [13]. Normally UCNs and photosensitizers are hydrophobic. Hydrophilic modification of UCNs and photosensitizers is a fundamental prerequisite for PDT applications. There are different strategies for surface modification of UCNs and photosensitizers, such as silica coating, ligand exchange by small molecules, polymer coating and so on [14–16]. Among these strategies, amphiphilic polymer coating is a convenient method to transfer hydrophobic substances to aqueous solution and keep them stable in water.

A variety of polymers have been developed to form a stable protective shield around these hydrophobic substance. Among these polymers, dextran is a naturally occurring polymer consisting of glucose monomers. Dextran is a suitable candidate for the construction of a delivery system for several reasons [17–19]. First, it is a biodegradable and biocompatible polysaccharide produced from mesenteroides; second, it has

hyperbranched structure which helps to decrease the nonspecific protein adhesion *in vivo*; third, it contains many accessible hydroxyl groups, which can be functionalized further with other molecules. Nevertheless, dextran is so hydrophilic and lacking in amphiphilic property that it is difficult to self-assemble into vesicles of very small size, which severely limits the application of dextran in delivery systems. So in order to transfer hydrophobic UCNs and photosensitizers into water by dextran, improving the amphiphilic property of dextran has become an urgent task.

In this work, amphiphilic lipid L- α -phosphatidylethanolamine, dioleoyl (DOPE), a common molecule for preparation of liposome [20], was grafted onto dextran to improve the amphiphilic property of dextran (see figure 1). Dextran-g-DOPE combines the advantages of both hydrophilic polymer and lipid molecule. To test the property of self-assembly into vesicles, dextran-g-DOPE was used for surface modification of UCNs and photosensitizers. Then dextran-g-DOPE, NaYF₄ (Y:Yb:Er = 78%:20%:2%) UCN and zinc phthalocyanine (ZnPc) were self-assembled into ZnPc loaded/dextran-g-DOPE nanocomplex by the thin-layer evaporation method (see figure 2). To evaluate the performance of this nanocomplex, the properties, such as structure, morphology, size distribution, drug loading efficiency, drug leaking and singlet oxygen generation *in vitro* were evaluated. Further to this, drug uptake efficiency and PDT treatment effect were also evaluated *in vitro*.

2. Methods and materials

2.1. Materials

NaYF₄ (Y:Yb:Er = 78%:20%:2%) was synthesized in our lab. Dextran from *Leuconostoc* spp (*Mr* ~ 40 000), sodium periodate (NaIO₄), sodium cyanoborohydrate (NaBH₃-CN), L- α -phosphatidylethanolamine, dioleoyl (DOPE), zinc phthalocyanine (ZnPc), chloroform, 9,10-anthracenediyl-bis (methylene) dimalonic acid (ABDA) and pyridine were purchased from Sigma-Aldrich. All other chemicals were of reagent grade and were used as received.

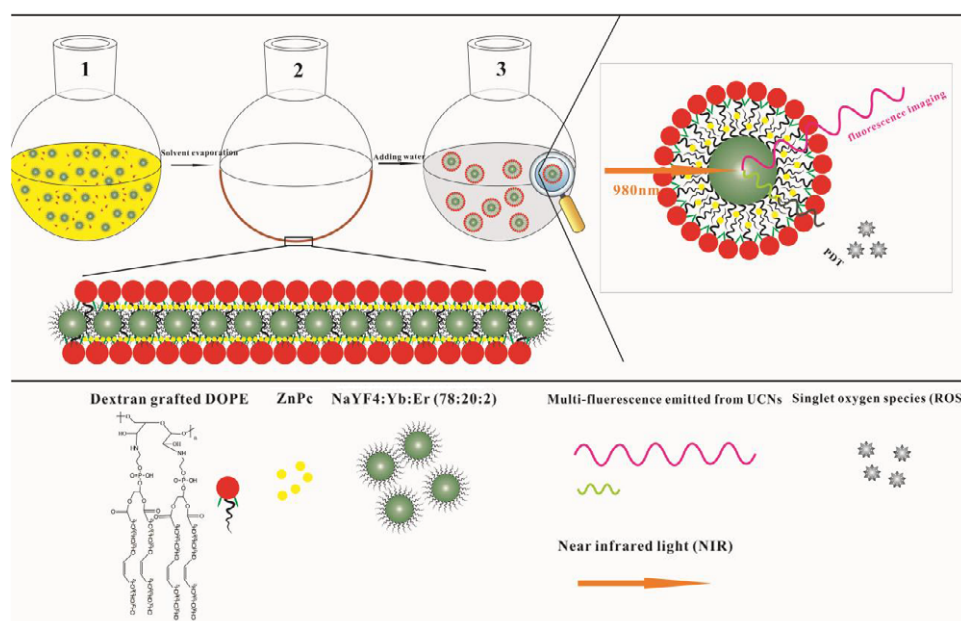


Figure 2. Schematic illustration of the thin-layer method for preparing the ZnPc loaded UCN/dextran-g-DOPE nanocomplex and of the nanocomplex for simultaneous imaging and PDT.

2.2. Synthesis of amphiphilic polymeric lipid molecule, DOPE grafted dextran (dextran-DOPE)

The synthesis procedure can be divided into two steps. As shown in figure 1, first NaIO_4 was used as oxidant to oxidize the hydroxyl groups on dextran into aldehyde groups for grafting DOPE lipid molecules [21]. For each sample, 80 ml of dextran aqueous solution (1 mg ml^{-1}) was added to a 100 ml round flask. Then, 10 mg NaIO_4 powder was dissolved into water and mixed with the dextran solution under stirring. The NaIO_4 oxidation of dextran to aldehyde functionalization was performed at 25°C for 24 h. Next, 20–30 mg NaBH_3CN was weighed into four separate 100 ml flasks under anhydrous conditions. After the appropriate oxidation time, the dextran solutions were transferred to the 100 ml flasks containing NaBH_3CN . After immediate mixing, 10 mg DOPE was added into the mixture. The graft reaction between DOPE and dextran lasted 24 h under stirring. After 24 h of stirring, the solution was purified by dialysis (8000 MW cutoff). The dialyzed solution was finally freeze-dried. FTIR was used to characterize the structure of amphiphilic polymeric lipid molecule DOPE grafted dextran.

2.3. Self-assembly of ZnPc loaded UCN/dextran-g-DOPE nanocomplex

NaYF_4 (Y:Yb:Er = 78%:20%:2%) nanocrystals were synthesized by thermal decomposition of rare-earth trifluoroacetates in the mixture of oleic acid and 1-octadecene using a well-established protocol [22]. The thin-layer evaporation method was used to transfer UCNs and ZnPc into the aqueous phase [23]. Briefly, 6–8 mg dextran-g-DOPE was dissolved in 1 ml of chloroform at room temperature. 1 ml stock solution of UCNs and different volume of ZnPc was mixed and added into the dextran-g-DOPE solution. Then chloroform was

evaporated with a vacuum rotary evaporator, and a thin film of polymeric lipid layers containing UCNs and ZnPc was formed on the wall of a 50 ml round bottomed flask. After that the lipid film was dispersed in deionized water under sonication at 30°C for 10 min. After centrifugation to remove the free ZnPc, the ZnPc loaded UCN/ dextran-g-DOPE nanocomplex was kept at 4°C .

2.4. Physicochemical characterization of ZnPc loaded UCN/ dextran-g-DOPE nanocomplex

2.4.1. Morphology test. The shape and morphology of the samples were observed via transmission electron microscopy (TEM). TEM observation of the NPs was carried out at an operating voltage of 200 kV with a 2010F in bright-field mode. Then a small amount of dilute suspensions of the samples were dropped onto a carbon-coated copper grid and air dried.

2.4.2. The structure analysis of dextran-g-DOPE by FTIR. FTIR spectra were recorded with KBr pellets on a IRPrestige-21 spectrometer. A spatula full of KBr was added into an agate mortar and ground to fine powder until no crystallites remained. Then a small amount of each powder sample (about of 0.1–2% of the KBr amount, or just enough to cover the tip of a spatula) was taken to mix with the KBr powder. Subsequently the mixture was ground for 3–5 min. After that the collar together with the pellet was put onto the sample holder.

2.4.3. ZnPc loading efficiency test. The unencapsulated free ZnPc was collected by centrifugation and the amount was calculated based on the UV absorbance at around 674 nm. The fluorescence spectrum was used to detect the emission peak

strength change of different samples. The loading efficiency (LE) of the process was calculated from

$$LE = \frac{M - M_1}{M + N} * 100\%$$

where M is the total amount of ZnPc added, M_1 is the amount of unencapsulated ZnPc, and N is the total weight of the UCNs and polymers added.

2.4.4. Fluorescence stability test in different pH buffer solution.

In order to test the fluorescence stability, the samples were kept in different pH buffer solution. At different time points, the fluorescence spectrum was measured by a Spectra Pro 2300i Fluorescence spectrophotometer (ACTON Research Corporation). The diluted samples were added into small cuvette. After 980 nm laser exposure, the spectrum was recorded from 350 to 700 nm.

2.4.5. Particle size test. The effective particle size was determined by Zetasizer Nano Series (Malvern Instruments Ltd) at room temperature. About 0.2 ml of each sample suspension was diluted with 2.5 ml of water immediately after preparation. The particle size was measured every hour to test the size stability in water.

2.4.6. Singlet oxygen test. Generation of singlet oxygen is usually detected by singlet oxygen sensors such as 9,10-anthracenediyl-bis (methylene) dimalonic acid (ABDA) [24]. Here the ABDA method was chosen to monitor the amount of singlet oxygen. In this method, ABDA can react with singlet oxygen to yield an endoperoxide and causes a decrease of ABDA absorption centered at 380 nm. Different samples were mixed with 1 mM ABDA and then irradiated by a 980 nm laser for different periods of time. The generation of singlet oxygen by different samples would result in the bleaching of ABDA absorption at 380 nm. The reduction of optical density at 380 nm thus reflects the production of 1O_2 .

2.5. Cell studies

2.5.1. Cell cultures. A human breast adenocarcinoma cell line (MCF-7 cells) purchased from American Type Culture Collection (ATCC, USA) was used for cell experiments. The MCF-7 cells were cultured in Dulbecco's Modified Eagle medium supplemented with 10% (v/v) fetal calf serum, penicillin and streptomycin. Cells were maintained at 37 °C in a humidified atmosphere containing 5% CO₂.

2.5.2. Cytotoxicity assay of different samples. CellTiter 96[®] AQueous One Solution Cell Proliferation Assay (MTS) was obtained from Promega and used to evaluate the potential cytotoxicity of samples in cancer cells. MCF-7 cells were seeded onto 96-well plates at 5000 cells/well. Following incubation for 24 h, samples with different concentration were added into the wells and incubated with the cells for 24 h. After 24 h, 20 μl of MTS assay solution per 100 μl of cell culture media was added into each well. After 1.5 h incubation at 37 °C, the plates were measured for absorbance at 490 nm. All test samples were assayed in triplicate and the cell viability was calculated.

2.5.3. Live and dead cell imaging. MCF-7 cells (20 000/well) were placed in 24-well plates. After 24 h, the culture medium was changed and cells were incubated with nanoparticles for another 24 h. Following this incubation, the wells were washed with sterile PBS (phosphate buffer solution, 1 ×) thrice. A stock solution containing 50 μl Calcein-AM and 33.3 μl propidium iodide per 5 ml PBS was prepared. Then, 500 μl of the staining solution was added to each well and the cells were incubated in the dark for 15 min. The wells were then washed once with PBS. Immediately, a bright-field image was taken followed by confocal imaging at 418 and 488 nm excitation of the same spot using a Nikon confocal laser scanning microscope. The bright-field and confocal images were then merged.

2.5.4. Cell uptake and ROS production of different samples.

MCF-7 cells were cultured in a 24-well plate for 24 h. Different samples with the same concentration of polymer were added to the plates and the cells were incubated for 24 h at 37 °C. ROS generated in cells were detected using an Image-iT LIVE Reactive Oxygen Species (ROS) Kit (Molecular Probes, OR, USA) as per the manufacturer's instructions. Briefly, the culture medium of cells that have been exposed to the different concentrations of UCNs were first replaced with HBSS containing 25 μM carboxy-H₂DCFDA and 0.1 μg ml⁻¹ DAPI to sufficiently cover the adhering cells. The cells were then subjected to photosensitization by 980 nm NIR laser irradiation for 30 min before they were washed thrice with plain HBSS. Fluorescent images of carboxy-H₂DCFDA, UCN and DAPI stainings on the cells were then promptly captured by excitation at 488, 980 and 408 nm respectively using a confocal laser scanning microscope specially fitted with a CW 980 nm laser excitation source.

2.5.5. Photodynamic therapy in vitro. After establishing its efficacy as a 1O_2 producer, we tested the nanoparticles for their PDT efficacy in inducing cell death. MCF-7 cells were seeded onto 96-well plates and incubated for 24 h. After cell attachment, different samples were added into the wells. After being cultured for 24 h, the cells in each well were exposed to 980 nm NIR light for 30 min. Cell viability was measured by MTS assay as described above.

3. Results and discussion

3.1. Synthesis procedure and structural characterization of dextran-grafted DOPE

Dextran, a polysaccharide consisting of 1,6- and partly 1,3-glucosidic linkages, has been extensively used in drug-delivery systems and biomedical devices. It comprises hydrophilic and colloidal biocompatible macromolecules, which are inert in biological systems and do not affect cell viability. Since dextran is fully water-soluble, it is necessary to improve the amphiphilic property for preparation of the drug carrier. In this work, L-α-phosphatidylethanolamine, dioleoyl (DOPE), a kind of amphiphilic lipid molecule for liposome, was selected to modify dextran because of its good amphiphilic property and

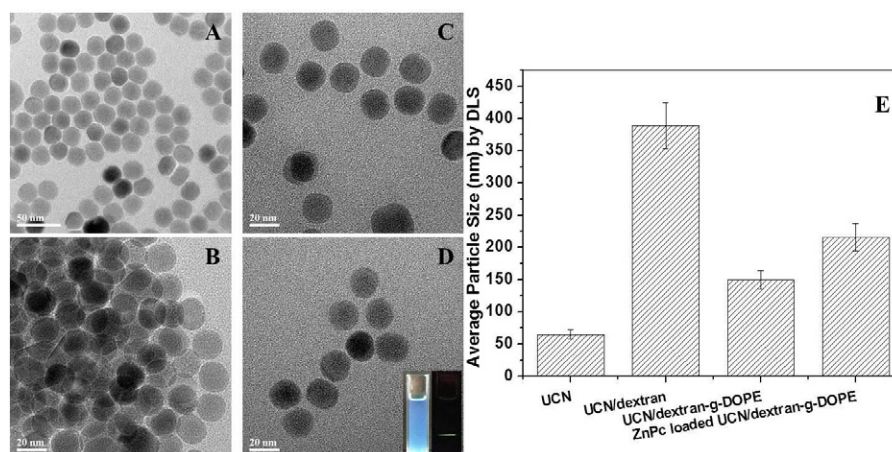


Figure 3. TEM images of NaYF₄:Yb, Er (Y:Yb:Er = 0.78:0.2:0.02) nanoparticles (A); UCN/dextran (B), UCN/dextran-g-DOPE nanocomplex (C), ZnPc loaded UCN/dextran-g-DOPE nanocomplex (D) (inset images: daylight photo and fluorescent photo of ZnPc loaded UCN/dextran-g-DOPE nanocomplex). The average particle sizes of different samples by DLS (E).

its use as a source of liposome which is one of the most popular drug-delivery systems. The synthesis procedure is shown in figure 1. As seen in figure 1, there were two steps in the grafting of DOPE onto the dextran. First, the hydroxyl groups on dextran were oxidized into aldehyde groups by NaIO₄. Then DOPE was grafted onto the dextran by the reaction between the aldehyde groups of oxidized dextran and the amine groups of DOPE.

The chemical structure of dextran-g-DOPE was tested by FTIR spectra (see figure 1(B)). Compared with the spectrum of pure dextran, in the spectrum of dextran-g-DOPE, the appearance of new intensive peaks at 2854.65 cm⁻¹, 1741.7 cm⁻¹ and 1465.9 cm⁻¹, respectively corresponded to C–H stretching vibration, C=O stretching vibration and C=C stretching vibration of DOPE, all of which indicated that the DOPE had been grafted onto the dextran successfully. In order to test the self-assembly ability, dextran-g-DOPE and dextran were dissolved into water and self-assembled into particles, respectively. Table S1 in the supporting information (available at stacks.iop.org/Nano/25/155103/mmedia) shows the particle size and zeta potential of the samples. As seen in table S1 (available at stacks.iop.org/Nano/25/155103/mmedia), the particle size of pure dextran was very large (4670 nm) with wide size distribution, which means that it is difficult to form small particles of dextran alone. Compared with pure dextran, the particle size of dextran-g-DOPE was much smaller (269 nm). Particle size results proved that the self-assembly property of dextran was improved by the grafting of DOPE.

3.2. Formulation of ZnPc loaded UCN/dextran-g-DOPE nanocomplex

After modification by DOPE, the amphiphilic property of dextran was improved markedly. Compared with pure dextran, dextran-g-DOPE not only can dissolve in water but also in organic solvent, such as dichloromethane and dichloromethane, which helps to expand the preparation method of nanoparticle based on dextran. In this work, the thin-layer evaporation

method was used to prepare the ZnPc loaded UCN/dextran-g-DOPE nanocomplex. As seen in figure 2, lipid polymer dextran-g-DOPE, UCNs and ZnPc were dissolved in chloroform at room temperature. Then chloroform was evaporated with a vacuum rotary evaporator, and a thin film of polymeric lipid layers containing UCNs and ZnPc was formed on the wall of the round bottomed flask. After that, the lipid film self-assembled into ZnPc loaded UCN/dextran-g-DOPE nanocomplex under sonication at 30 °C for 10 min. As seen in figure 2, upon NIR continuous wave (CW) laser excitation, two upconverting luminescence bands of UCNs, peaking around 540 and 650 nm, are employed for simultaneous PDT and fluorescence imaging, respectively. The ZnPc loaded UCN/dextran-g-DOPE nanocomplex will simultaneously meet the demands of high fluorescent intensity in imaging and high singlet oxygen production yield in PDT.

3.3. Characterization of ZnPc loaded UCN/dextran-g-DOPE nanocomplex

3.3.1. Morphology and particle size of these samples. The particle size and morphology of nanoparticles for drug delivery is one of the most important parameters that can affect the movement in and out of the vasculature and the uptake efficacy into tumor cells. TEM and DLS were used to characterize the morphology and particle size of these samples. The TEM images of different samples are shown in figure 3. The synthesized NaYF₄-based UCNs dispersed into individual ones of uniform small size (see figure 3(A)). The UCNs aggregated after being modified by the pure dextran, which indicated that the pure dextran cannot protect the UCNs in water effectively. As seen in figure 3(C), after UCNs were transferred into water by dextran-g-DOPE, these UCNs still dispersed as individuals with the small particle size without aggregation. When ZnPc was loaded into the UCN/dextran-g-DOPE, the size and morphology showed nearly no change compared with the UCN/dextran-g-DOPE nanocomplex in figure 3(C). The distance between individual UCNs was enlarged after modification by dextran-DOPE (see figures 3(C)–(D)). The

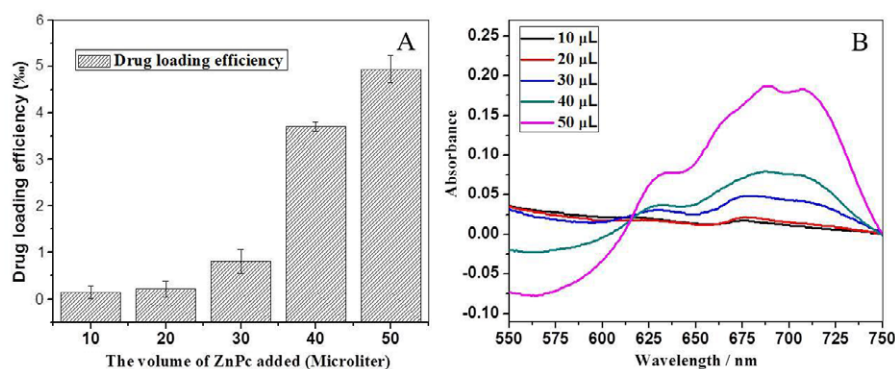


Figure 4. (A) ZnPc loading efficiency of different samples and (B) UV-vis spectrum changes of ZnPc loaded UCN/dextran-DOPE nanocomplex by changing the amount of ZnPc added during the preparation process.

reason may be that the lipid polymer layer has high negative charge (see table S1 available at stacks.iop.org/Nano/25/155103/mmedia), which helped to repel the nanoparticles from each other and keep them stable. The particle size and zeta potential of the UCNs, UCN/dextran-DOPE, and ZnPc loaded UCN/dextran-g-DOPE were measured by dynamic light scattering (see figure 3(E)). The results show that the effective size of ZnPc loaded UCN/dextran-g-DOPE is 216 nm, which is a little larger than that of UCN/dextran-g-DOPE without loading ZnPc.

3.3.2. ZnPc loading test. The drug loading efficiency is defined as the weight percentage of ZnPc in nanoparticles relative to the initial feeding amount of ZnPc. UV-vis spectra were used to test the absorbance of ZnPc for calculating the drug loading efficiency. The spectra of UCN/dextran-g-DOPE nanoparticles loaded with different amounts of ZnPc are shown in figure 4(B). It was found that the characteristic absorption peak strength of ZnPc at 674 nm increased with increased amount of ZnPc added. From the absorption data, the drug loading efficiency was calculated. As shown in figure 4(A), along with the increase of ZnPc added, the loading capacity increased and reached 4.94% (w/w) at volumes above 50 ml. In order to maintain the encapsulation ratio, the amount of ZnPc added was fixed at 50 ml in the next experiment.

3.3.3. Fluorescence stability of ZnPc loaded UCN/dextran-g-DOPE nanocomplex in various buffer solutions at different pH condition. Fluorescent quenching of fluorescent probes in buffer solution is a common problem during application. Fluorescence stability directly influences the effect of fluorescence imaging *in vivo* and *in vitro*. Here the fluorescence spectra were used to observe the fluorescence intensity changes of ZnPc loaded UCN/dextran-g-DOPE nanocomplex kept in various buffer solutions at different pH conditions. The fluorescence spectrum results are shown in figure 5. The fluorescence stability of ZnPc loaded UCN/dextran-g-DOPE nanocomplex was evaluated under different pH condition (7.4, 6.3 and 8.3) and buffers (SSC buffer, EDTA buffer and PBS). As seen in figure 6(A), the fluorescence intensity at 543 nm declined by 5% after storage in water for 6 h. When the samples were stored in different buffers (SSC, EDTA and PBS at pH 7.4 and PBS at

pH 8.3), the fluorescence intensity at 543 nm declined by 7%, 7.5%, 9% and 6.7%, respectively after 6 h (figures 6(B)–(D)), which is nearly the same as when stored in water. After storage in PBS at pH 6.3, the fluorescence intensity decrement of samples is about 38%, which is much higher than when stored at pH 7.4 and 8.3. These results indicate that when stored in buffers at pH 7.4 and 8.3, the dextran-g-DOPE polymeric lipid shell can keep UCNs stable and effectively protect them from hydroxyl ion corrosion. But with decreasing pH value, there are more and more hydroxyl ions in the buffers, which erode the UCNs and cause fluorescent quenching. Hence, the UCN/dextran-g-DOPE nanocomplex was quite stable in buffers except in acid condition.

3.3.4. Detection of singlet oxygen generation (ROS). There are two key steps in the photodynamic process: first, the photosensitizer ZnPc was excited by the upconverting fluorescence emitted from UCNs. Then, the energy absorbed by ZnPc was transferred to triplet oxygen for production of reactive singlet oxygen (ROS) to kill cancer cells. To prove the energy transfer from the UCNs to ZnPc, the fluorescence emission spectra were measured. As seen in figure 6(A), with the increase in the amount of ZnPc added, the red fluorescence emitted from the UCNs was quenched significantly which indicated that the energy was transferred from the UCNs to ZnPc successfully.

Singlet oxygen ($^1\text{O}_2$) is a higher-energy state molecular oxygen species. It is one of the most active intermediates involved in chemical and biochemical reactions. ZnPc can be excited to produce reactive singlet oxygen species which cause detrimental oxidation of biomolecules in cancer cells [25, 26]. To assess the capability of singlet oxygen generation of the samples, ABDA was employed as a probe molecule to monitor the singlet oxygen generation. As seen in figure 6(B), in the three control groups (ZnPc loaded UCN/dextran-g-DOPE group without NIR laser irradiation, pure ZnPc group with NIR laser irradiation and UCN/dextran-g-DOPE group with NIR laser irradiation) the absorbance of ABDA shows nearly no change, which means that these three groups are not able to generate $^1\text{O}_2$, while for the ZnPc loaded UCN/dextran-g-DOPE noncomplex group with 980 nm laser exposure, the absorbance of ABDA decreased significantly, all of which indicates that the ZnPc, UCN/dextran-g-DOPE and NIR irradiation are all essential to the ROS production.

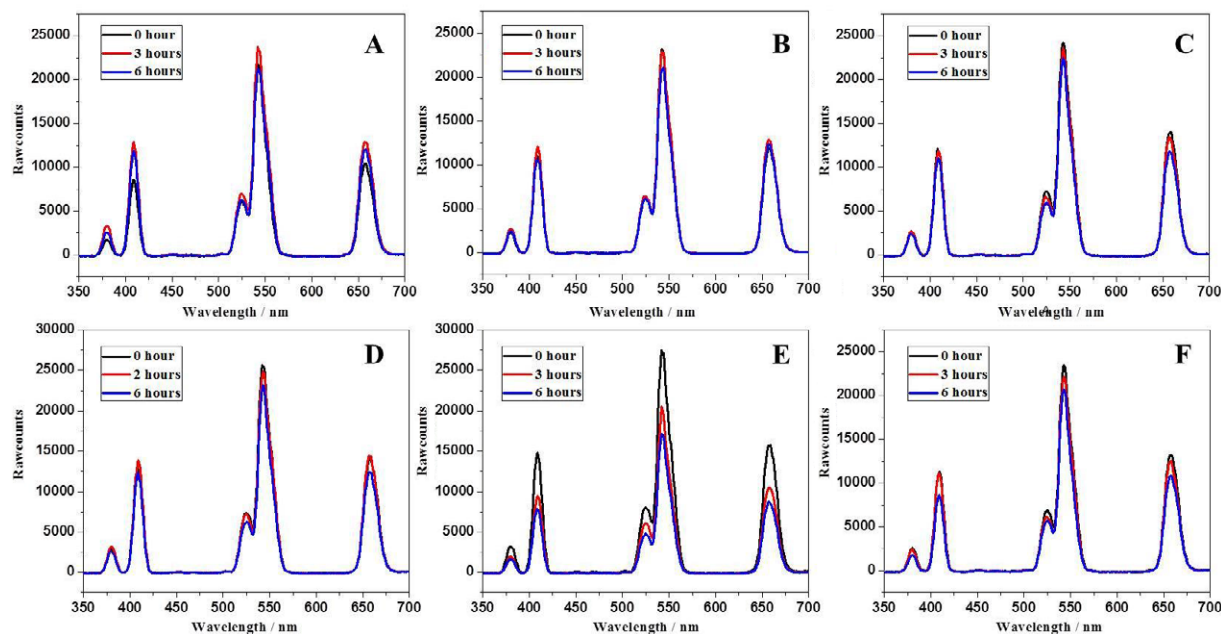


Figure 5. The fluorescence stability of UCN/dextran-g-DOPE nanocomplex in water (A), SSC buffer at pH 7.4 (B), EDTA buffer at pH 7.4 (C), PBS buffer 7.4 (D), PBS buffer at pH 6.3 (E) and PBS buffer at pH 8.3 (F).

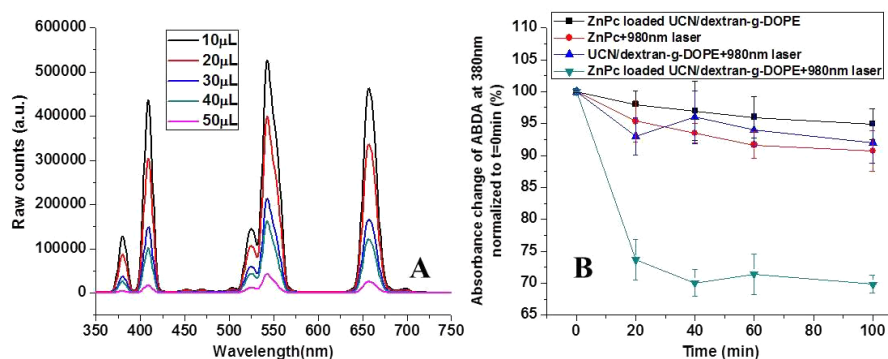


Figure 6. The fluorescence emission spectra of different samples with various ZnPc (A) and the ROS production test of ZnPc loaded UCN/dextran-DOPE nanocomplex within 100 min (B).

3.4. Cytotoxicity study

The cytotoxicity of the different samples was preliminarily estimated by MTS assays on MCF-7 cells. The results are shown in figure 7. The cytotoxic activity was evaluated ranging from 10 to 100 $\mu\text{g ml}^{-1}$. We compared the ZnPc loaded UCN/dextran-g-DOPE group with UCN/dextran-g-DOPE group and pure dextran-g-DOPE group. As seen in figure 7, the ZnPc loaded UCN/dextran-g-DOPE group did not cause significant cytotoxicity against the cell line at concentration under 20 $\mu\text{g ml}^{-1}$. Interestingly, with the increase in concentration from 50 to 100 $\mu\text{g ml}^{-1}$, the ZnPc loaded UCN/dextran-g-DOPE group showed lower cytotoxicity than the other groups. In the cell study, the concentration of different samples was set at 20 $\mu\text{g ml}^{-1}$ to ensure cell viability. In order to double check the cell viability at this concentration, the live cells were labeled with green fluorescent dye and the dead cells were labeled with red fluorescent dye. As seen in figures 7(B)–(C), after incubation with these three groups at

20 $\mu\text{g ml}^{-1}$, most of the cells show green fluorescence which indicates that under 20 $\mu\text{g ml}^{-1}$, most cells remained alive.

3.5. Cell uptake and singlet oxygen production of different samples

For the purpose of killing cancer cells, nontoxic light-sensitive ZnPc needs to sneak into the cancer cells first. It then produces ROS, singlet oxygen after excitation by light, which is toxic to the biomolecules in cells. So the photodynamic effect is related directly to the rate of cell uptake and singlet oxygen production. To monitor the intracellular uptake and singlet oxygen production, MCF-7 cells were incubated with different samples for 4 h. In order to evaluate the ability of the UCNs to generate $^1\text{O}_2$, the dye 9,10-anthracenediyl-bis (methylene) dimalonic acid as an acceptor of $^1\text{O}_2$ was added into the cells. After washing the unbound nanoparticles and dyes, the cell were observed in bright field and fluorescence field by a confocal microscope equipped with a 980 nm NIR laser.

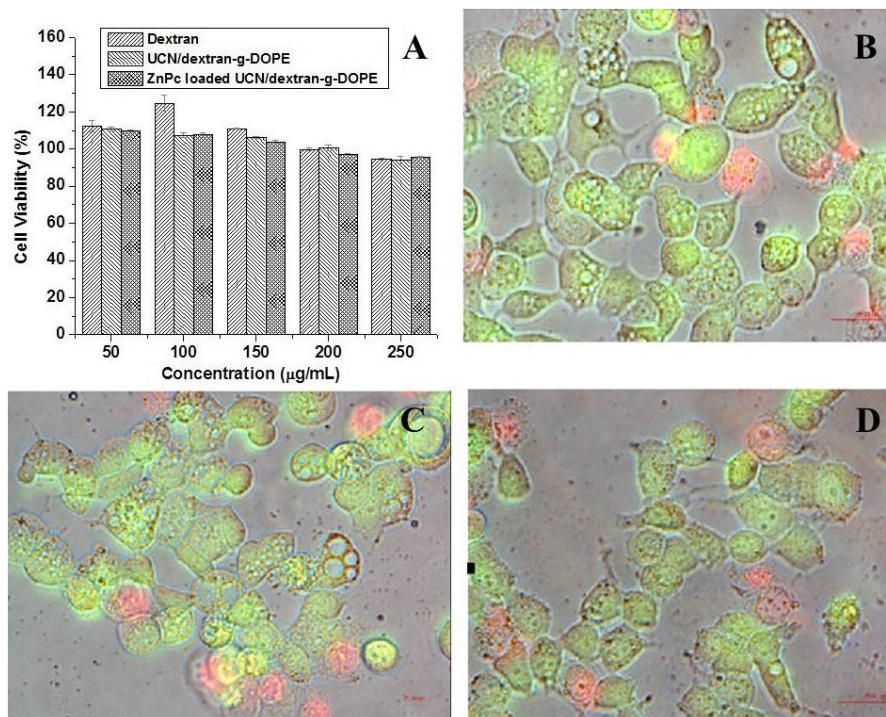


Figure 7. Cell toxicity (A); live and dead cell imaging of (concentration of samples: $250 \mu\text{g ml}^{-1}$) dextran-g-DOPE group (B), UCN/dextran-g-DOPE group (C) and ZnPc loaded UCN/dextran-g-DOPE group (D).

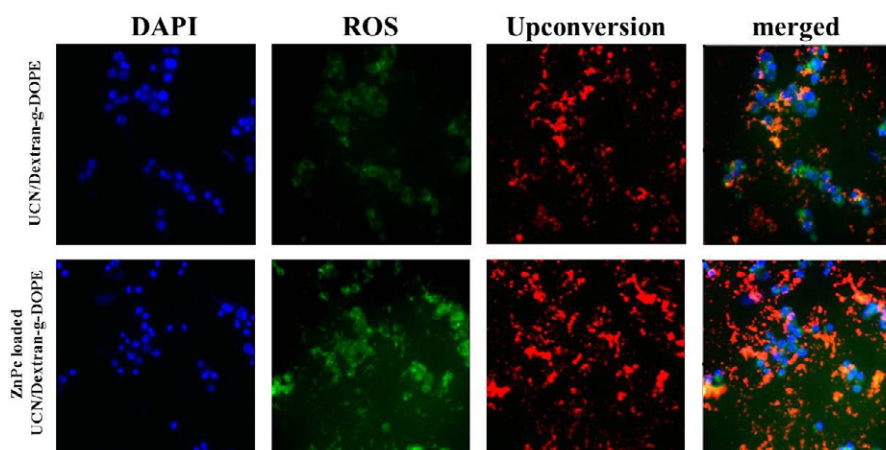


Figure 8. Cell uptake and ROS generation test. The positions of the cells are indicated by blue fluorescence indicative of nuclear counterstaining with DAPI (blue color); green fluorescence represents carboxy- H_2DCFDA marker for detection of ROS; red fluorescence represents UCNs.

As seen in figure 8, obvious red upconverting luminescence from the UCNs at 980 nm excitation and green fluorescence of ABDA marker for ROS were simultaneously observed in the cancer cells. The merged images indicate that the fluorescence of UCNs and green fluorescence of ABDA marker for ROS co-existed in the cells, mainly appearing in the cytoplasmic regions. Compared with UCN/dextran-g-DOPE group without loading ZnPc, there was much stronger green fluorescence in the ZnPc loaded UCN/dextran-g-DOPE, which proves that the energy emitted from the UCN at 980 nm excitation successfully transferred to the photosensitizer.

3.6. PDT effects test on cancer cells by MTS

The ultimate goal for PDT treatment is to kill cancer cells *in vitro*. So the efficacy of the PDT treatment was assessed by measuring cell viability using MTS assay. Figure 9 shows the cell viability. The viability of control cells without NIR treatment was set as 100% viability. As seen in figure 9, the cell viability is only 29.15% in ZnPc loaded UCN/dextran-g-DOPE group with NIR irradiation, which is much lower than that in UCN/dextran-g-DOPE group without loading ZnPc. These results implied that UCN/dextran-g-DOPE has no treatment effect before combining with photosensitizer

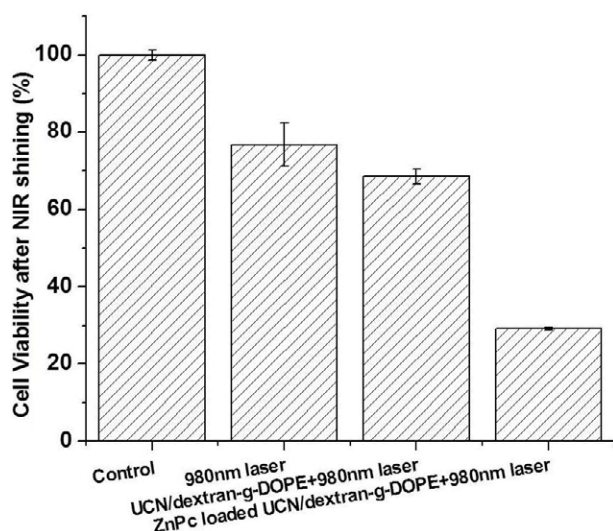


Figure 9. PDT treatment efficiency on MCF-7 cells, showing the results for three control groups of untreated cells, cells treated with NIR laser, and cells treated with UCN/dextran-g-DOPE nanocomplex plus NIR laser, and one experiment group of cells treated with ZnPc loaded UCN/dextran-DOPE nanocomplex plus NIR laser.

ZnPc, which further proves that ZnPc can be excited by the high-energy photon emitted from UCNs successfully to produce singlet oxygen for inducing cell death.

4. Conclusions

In summary, a new kind of amphiphilic DOPE modified dextran (dextran-DOPE) was synthesized successfully. In aqueous solutions, dextran-g-DOPE can self-assemble into micelles. Based on amphiphilic dextran-DOPE, UCN/dextran-g-DOPE nanocomplex, as a new photosensitizer carrier for PDT, was prepared via a thin-layer evaporation approach. It has been demonstrated that this kind of nanocomplex has nanosize with narrow size distribution. ZnPc can be loaded into this kind of nanocomplex through hydrophobic interactions. The cell uptake results suggested that the co-delivery of UCNs and ZnPc inside the cells ensured that the fluorescence from the UCNs excited by NIR can effectively activate the photosensitizer ZnPc to generate cytotoxic singlet oxygen. In PDT tests, the ZnPc loaded UCN/dextran-g-DOPE nanocomplex has much better treatment effect on the tumor cells *in vitro*. In conclusion, the ZnPc loaded UCN/dextran-g-DOPE nanocomplex may be suitable as a potential drug-delivery system for PDT based on the upconverting mechanism.

Acknowledgments

The authors gratefully acknowledge the National High Technology Program of China (863 Program) (2012AA022603), the National Natural Science Foundation of China (51303126, 51373117 and 81070871), the Key Project of Tianjin Natural Science Foundation (13JCZDJC33200) and the Doctoral Base Foundation of the Educational Ministry of China (20120032110027).

References

- [1] Konan Y N, Gurny R and Allemann E 2002 State of the art in the delivery of photosensitizers for photodynamic therapy *J. Photochem. Photobiol. B* **66** 89–106
- [2] Schuitmaker J J, Bass P, van Leengoed H, van der Meulen F W, Star W M and van Zandwijk N 1996 Photodynamic therapy: a promising new modality for the treatment of cancer *J. Photochem. Photobiol. B* **34** 3–12
- [3] Palumbo G 2007 Photodynamic therapy and cancer: a brief sightseeing tour *Expert Opin. Drug Discovery* **4** 131–48
- [4] Hsi R A, Rosenthal D I and Glatstein E 1999 Photodynamic therapy in the treatment of cancer—current state of the art *Drugs* **57** 725–34
- [5] MacDonald I J and Dougherty T J 2001 Basic principles of photodynamic therapy *J. Porphyrins Phthalocyanines* **5** 105–29
- [6] Wang C, Tao H Q, Cheng L and Liu Z 2011 Near-infrared light induced *in vivo* photodynamic therapy of cancer based on upconversion nanoparticles *Biomaterials* **32** 6145–54
- [7] Idris N M, Gnanasammandhan M K, Zhang J, Ho P C, Mahendran R and Zhang Y 2012 *In vivo* photodynamic therapy using upconversion nanoparticles as remote-controlled nanotransducers *Nature Med.* **18** 1580
- [8] Frangioni J V 2003 *In vivo* near-infrared fluorescence imaging *Curr. Opin. Chem. Biol.* **7** 626–34
- [9] Auzel F 2004 Upconversion and anti-Stokes processes with *f* and *d* ions in solids *Chem. Rev.* **104** 139–73
- [10] Liu Z, Sun L, Li F, Liu Q, Shi L, Zhang D, Yuan S, Liu T and Qiu Y 2011 One-pot self-assembly of multifunctional mesoporous nanoprobe with magnetic nanoparticles and hydrophobic upconversion nanocrystals *J. Mater. Chem.* **21** 17615–8
- [11] Sun L-N, Peng H, Stich M I, Achatz D and Wolfbeis O S 2009 pH sensor based on upconverting luminescent lanthanide nanorods *Chem. Commun.* **33** 5000–2
- [12] Wei Z, Sun L, Liu J, Zhang J Z, Yang H, Yang Y and Shi L 2014 Cysteine modified rare-earth up-converting nanoparticles for *in vitro* and *in vivo* bioimaging *Biomaterials* **35** 387–92
- [13] Cui S S, Yin D Y, Chen Y Q, Di Y F, Chen H Y, Ma Y X, Achilefu S and Gu Y Q 2013 *In vivo* targeted deep-tissue photodynamic therapy based on near-infrared light triggered upconversion nanoconstruct *ACS Nano* **7** 676–88
- [14] Guerrero-Martinez A, Perez-Juste J and Liz-Marzan L M 2010 Recent progress on silica coating of nanoparticles and related nanomaterials *Adv. Mater.* **22** 1182–95
- [15] Allen C, Maysinger D and Eisenberg A 1999 Nano-engineering block copolymer aggregates for drug delivery *Colloids Surf. B* **16** 3–27
- [16] Caruso F 2001 Nanoengineering of particle surfaces *Adv. Mater.* **13** 11–22
- [17] Mehvar R 2000 Dextran for targeted and sustained delivery of therapeutic and imaging agents *J. Control. Release* **69** 1–25
- [18] Bisht S and Maitra A 2009 Dextran-doxorubicin/chitosan nanoparticles for solid tumor therapy *Wiley Interdiscip. Rev. Nanomed. Nanobiotechnol.* **1** 415–25
- [19] Varshosaz J 2012 Dextran conjugates in drug delivery *Expert Opin. Drug Discovery* **9** 509–23
- [20] Maitani Y, Igarashi S, Sato M and Hattori Y 2007 Cationic liposome (DC-Chol/DOPE=1:2) and a modified ethanol injection method to prepare liposomes, increased gene expression *Int. J. Pharm.* **342** 33–9

- [21] Miksa D, Irish E R, Chen D, Composto R J and Eckmann D M 2006 Dextran functionalized surfaces via reductive amination: morphology, wetting, and adhesion *Biomacromolecules* **7** 557–64
- [22] Li Z Q and Zhang Y 2006 Monodisperse silica-coated polyvinylpyrrolidone/NaYF₄ nanocrystals with multicolor upconversion fluorescence emission *Angew. Chem. Int. Edn* **45** 7732–5
- [23] Wang H J, Zhao P Q, Su W Y, Wang S, Liao Z Y, Niu R F and Chang J 2010 PLGA/polymeric liposome for targeted drug and gene co-delivery *Biomaterials* **31** 8741–8
- [24] Zhao T T, Wu H, Yao S Q, Xu Q H and Xu G Q 2010 Nanocomposites containing gold nanorods and porphyrin-doped mesoporous silica with dual capability of two-photon imaging and photosensitization *Langmuir* **26** 14937–42
- [25] Yano S, Hirohara S, Obata M, Hagiya Y, Ogura S, Ikeda A, Kataoka H, Tanaka M and Joh T 2011 Current states and future views in photodynamic therapy *J. Photochem. Photobiol. C* **12** 46–67
- [26] Bae B C and Na K 2012 Development of polymeric cargo for delivery of photosensitizer in photodynamic therapy *Int. J. Photoenergy* **2012** 431975